PLOS ONE

RESEARCH ARTICLE

Serum Amyloid P inhibits single stranded RNA-induced lung inflammation, lung damage, and cytokine storm in mice

Tejas R. Karhadkar[☯], **Darrell Pilling**[☯], **Richard H. Gomer***

Department of Biology, Texas A&M University, College Station, Texas, United States of America

☯ These authors contributed equally to this work.
* rgomer@tamu.edu

Citation: Karhadkar TR, Pilling D, Gomer RH (2021) Serum Amyloid P inhibits single stranded RNA-induced lung inflammation, lung damage, and cytokine storm in mice. PLoS ONE 16(1): e0245924. https://doi.org/10.1371/journal.pone.0245924

Editor: Heinz Fehrenbach, Forschungszentrum Borstel Leibniz-Zentrum fur Medizin und Biowissenschaften, GERMANY

Received: August 21, 2020

Accepted: January 9, 2021

Published: January 22, 2021

Data Availability Statement: All relevant data are within the manuscript and its Supporting information files.

Funding: This work was supported by National Institute of Health HL-132919 and NIH GM118355-03S1 (Both grants to RHG). www.nih.gov The funders had no role in study design, data collection and analysis, decision to publish, or preparation of the manuscript.

Abstract

SARS-CoV-2 is a single stranded RNA (ssRNA) virus and contains GU-rich sequences distributed abundantly in the genome. In COVID-19, the infection and immune hyperactivation causes accumulation of inflammatory immune cells, blood clots, and protein aggregates in lung fluid, increased lung alveolar wall thickness, and upregulation of serum cytokine levels. A serum protein called serum amyloid P (SAP) has a calming effect on the innate immune system and shows efficacy as a therapeutic for fibrosis in animal models and clinical trials. Here we show that aspiration of the GU-rich ssRNA oligonucleotide ORN06 into mouse lungs induces all of the above COVID-19-like symptoms. Men tend to have more severe COVID-19 symptoms than women, and in the aspirated ORN06 model, male mice tended to have more severe symptoms than female mice. Intraperitoneal injections of SAP starting from day 1 post ORN06 aspiration attenuated the ORN06-induced increase in the number of inflammatory cells and formation of clot-like aggregates in the mouse lung fluid, reduced ORN06-increased alveolar wall thickness and accumulation of exudates in the alveolar airspace, and attenuated an ORN06-induced upregulation of the inflammatory cytokines IL-1β, IL-6, IL-12p70, IL-23, and IL-27 in serum. SAP also reduced D-dimer levels in the lung fluid. In human peripheral blood mononuclear cells, SAP attenuated ORN06-induced extracellular accumulation of IL-6. Together, these results suggest that aspiration of ORN06 is a simple model for both COVID-19 as well as cytokine storm in general, and that SAP is a potential therapeutic for diseases with COVID-19-like symptoms and/or a cytokine storm.

Introduction

Coronavirus disease 2019 (COVID-19) is generally caused by inhalation of the severe acute respiratory syndrome coronavirus 2 (SARS-CoV-2), a single-stranded RNA (ssRNA) virus related to severe acute respiratory syndrome coronavirus (SARS-CoV) and Middle East respiratory syndrome-related coronavirus (MERS-CoV) [1]. Human patients and murine models of SARS-CoV, MERS, and SARS-CoV2 indicate that severe disease may be triggered by a cytokine storm, in which, as in other cytokine storm associated diseases, an over exuberant production of cytokines leads to the accumulation of immune cells in sensitive organs such as the lungs [2,3]. Although there are similar numbers of confirmed SARS-CoV2 cases between men

Competing interests: I have read the journal's policy and the authors of this manuscript have the following competing interests: Texas A&M University has a patent application on the use of SAP to treat cytokine storm and COVID-19-associated lung inflammation and lung damage. DP, TRK, and RHG are inventors on this patent application. This does not alter our adherence to PLOS ONE policies on sharing data and materials.

and women, severe COVID-19 disease, as measured by hospitalization, admission to intensive care units, and rates of mortality, are 1.5 to 2 times higher in men than women [4–6]. These data are independent of other known factors, such as smoking, diabetes, obesity, heart disease, chronic kidney disease, or chronic lung disease [6,7].

Lung biopsy and autopsy findings indicate that COVID-19 is associated with an accumulation of **cell**-free protein-rich exudate in the alveoli, alveolar wall thickening, and inflammation (accumulation of immune cells) [8–13]. COVID-19 patients are also at risk of disseminated intravascular coagulation and deposition of fibrin clots in the lungs [8,9,12–14]. In both animal models and COVID-19 patients, there is a consistent accumulation of macrophages in the lungs, whereas increased numbers of lung neutrophils appear to be associated with comorbidities such as pneumonia [12,15,16].

Serum amyloid P (SAP; PTX2) is a member of the pentraxin family of proteins that includes C-reactive protein (CRP; PTX1) and pentraxin-3 (PTX3). SAP is made by hepatocytes and secreted into the blood [17,18]. SAP binds to a variety of molecules including DNA and apoptotic debris, bacterial polysaccharides, amyloid deposits, and bacterial and viral proteins [19–21]. Phagocytic cells such as monocytes and macrophages then bind the SAP and engulf the debris or other material the pentraxin has bound [22]. SAP binds to Fc receptors (receptors for IgG) as well as the C-type lectin receptor DC-SIGN/CD209 on monocytes and macrophages [22–26], and inhibits the formation of pro-inflammatory and pro-fibrotic macrophages, and promotes the formation of immuno-regulatory macrophages [27–36]. In addition to promoting the formation of immuno-regulatory macrophages, SAP induces macrophages to secrete the anti-inflammatory cytokine IL-10 [31,32,37]. SAP decreases neutrophil binding to extracellular matrix components [38–40], and in a mouse model of lung inflammation, SAP injections starting 24 hours after insult reduced the number of neutrophils in the lungs [40]. In animal models and human clinical trials, SAP inhibits fibrosis [28,32,41–43]. SAP is also effective as an inhibitor of influenza A virus infections [44–46].

Cells can sense the presence of the SARS-CoV-2 ssRNA virus using the ssRNA-sensitive intracellular toll-like receptors TLR7 and TLR8 [47,48]. Adding GU-rich ssRNAs to human peripheral blood immune cells induces proinflammatory cytokine production, and tail vein injections of GU-rich ssRNAs in mice lead to pulmonary edema, accumulation of inflammatory cells, and alveolar hemorrhage/damage in the lung [47,49].

In this report, we show that oropharyngeal aspiration of ORN06 induces a cytokine storm and lung damage in mice with similarities to the cytokine storm and lung damage seen in patients infected with the ssRNA viruses SARS-CoV-2, including more severe effects in male mice than female mice. We find that SAP strongly attenuates the ORN06 effects, suggesting that SAP could be a potential therapeutic for severe ssRNA virus infections and possibly cytokine storms in general.

Materials and methods

Preparation of SAP

Purified human SAP (30C-CP1104LY) was purchased from Fitzgerald Industries (Acton, MA). Before use, the SAP was buffer exchanged into 20 mM sodium phosphate, pH 7.4 to remove sodium azide and EDTA present in the commercial preparation. The SAP was diluted 1:1 with 20 mM sodium phosphate, pH 7.4, and added to Amicon Ultra 0.5ML 10 kDa cutoff centrifugal filter units (Millipore-Sigma, Burlington, MA) and centrifuged at 10,000 x g for 10 minutes. The SAP in the upper reservoir was then resuspended with 0.4 ml 20 mM phosphate buffer and centrifuged again. This process was repeated four times to exchange the buffer to 20 mM sodium phosphate. Buffer-exchanged preparations were then checked for protein

concentration by OD 260/280/320 using a Take3 micro-volume plate with a SynergyMX plate reader (BioTek, Winooski, VT, USA) as previously described [50]. The SAP, at 2.5–4 mg/ ml, was stored in aliquots at 4˚C and used within 14 days. SDS-PAGE of 1 μg of this SAP showed a single band at the expected molecular mass of 26 kDa (S1 Fig).

Mouse model of lung damage and cytokine storm

This study was carried out in strict accordance with the recommendations in the Guide for the Care and use of Laboratory Animals of the National Institutes of Health. The protocol was approved by Texas A&M University Animal Use and Care Committee approved the protocol (Protocol Number: IACUC 2017–0414). 5-week old 20 g male and female C57BL/6 mice (Jackson Laboratories, Bar Harbor, ME) were given an oropharyngeal aspiration of 1 mg/kg (or less where indicated) ORN06/LyoVec (a ssRNA oligonucleotide with 6 UGU repeats complexed with a lipid which protects the ssRNA from degradation; henceforth referred to as ORN06) (InvivoGen, San Diego, CA) in 50 μl phosphate-buffered saline (PBS), or an oropharyngeal aspiration of an equal volume of PBS as a control, following [51,52]. At 24 and 48 hours after ORN06 insult, the control mice and some of the ORN06-treated mice were given intraperitoneal injections of 100 μl PBS, or SAP diluted to a dose of 2.5 mg/kg in 100 μl PBS. All the mice were monitored twice daily to observe any sign of distress. At day 3, mice were euthanized by CO_2 inhalation, and bronchoalveolar lavage fluid (BALF) was obtained as previously described [34,51]. All mice survived until euthanasia at day 3, and 20 mice were used in the study.

Staining of bronchoalveolar lavage fluid (BALF) cells

BALF cells were counted and processed to prepare cell spots as described previously [40,53]. In brief, the primary BALF cells were collected by centrifugation at 500 × g for 10 min. Primary BALF cell pellets were resuspended in the secondary and tertiary BAL fluid and the combined cells were collected by centrifugation at 500 × g for 5 min. The cells were resuspended in 500 μl 2% BSA-PBS and counted with a hemocytometer. Cells (100 μl) were then resuspended in 2% BSA-PBS and cell spots were put onto glass slides (Superfrost Plus white slides; VWR Scientific, West Chester, PA) and then air-dried. After air drying for 48 hours at room temperature, some of the prepared BALF cell spots were fixed and treated with Wright-Giemsa stain (Polysciences, Inc., Warrington, PA) following the manufacturer's instructions. At least 150 cells per mouse were examined and quantified for cell type following the manufacturer's instructions using a CME microscope (Leica, Buffalo Grove, IL) with a 40x objective, and selected areas were imaged with a 100x oil immersion objective on an Eclipse Ti2 microscope (Nikon, Melville, NY) with a 10 megapixel color CCD camera (Amscope, Irvine, CA).

Immunochemistry on BALF cell spots and counts of cells was performed as described previously [34,54,55]. Slides were incubated with 5 μg/mL of monoclonal antibodies overnight at 4˚C using anti-CD3 (100202, clone 17A2, BioLegend, San Diego, CA) to detect T-cells, anti-CD11b (101202, clone M1/70, BioLegend) to detect blood and inflammatory macrophages, anti-CD11c (M100-3, clone 223H7, MBL International, Woburn, MA) to detect alveolar macrophages and dendritic cells, anti-CD45 (103102, clone 30-F11, BioLegend) for total leukocytes, anti-Ly6G (127602, clone 1A8, BioLegend) to detect neutrophils, with isotype-matched irrelevant rat antibodies (400501, clone RTK2758 and 400602, clone RTK4530, BioLegend) as controls, diluted to 5 μg/ml in PBS containing 2% (w:v) Fraction V BSA bovine serum albumin (PBS-BSA) (VWR, Radnor, PA). Slides were then washed in PBS, with 6 changes of PBS over 30 minutes, and then incubated with 1 μg/ml biotin-conjugated F(ab')2-donkey anti-rat antibodies (Novus Biologicals, Littleton, CO) in PBS-BSA for 30 minutes at room temperature. Slides were washed as above and then incubated with 1:1000 streptavidin-conjugated alkaline

phosphatase (Vector Laboratories, Burlingame, CA) in PBS-BSA for 30 minutes and washed as above. Staining was developed with the Vector Red Alkaline Phosphatase Kit (Vector Laboratories) for 4 minutes at room temperature following the manufacturer's directions. Cells were counterstained with Gill's hematoxylin #3 (Sigma-Aldrich, St. Louis, MO), air dried overnight, and then coverslip (VWR) mounted in Permount mounting medium (17986–01, Electron Microscopy Sciences, Hatfield, PA). Using a 40x objective, at least 100 cells from each stained BALF spot were examined and the percent positive cells was recorded.

Lung histology

After collecting BALF, the lungs from the mice were harvested and inflated with Surgipath frozen section compound (#3801480, Leica, Buffalo Grove, IL), frozen on dry ice, and stored at -80˚C. 10 μm cryosections of lungs were placed on Superfrost Plus glass slides (VWR) and were air dried for 48 hours. The slides were fixed in acetone for 20 minutes, and then air dried. Slides were incubated for 5 minutes in water at room temperature and then stained for two minutes at room temperature with Gill's hematoxylin No. 3 solution (Sigma-Aldrich, St. Louis, MO) diluted 1:3 with water and then rinsed under tap water for 1 minute at room temperature. The slides were then incubated with 0.1% eosin for 1 minute and then washed by dipping in water for 10 seconds. The stained slides were allowed to air dry for 2 hours; cleared with xylenes (VWR); and mounted with Permount mounting medium (Electron Microscopy Sciences). After drying the mounted slides for 48 hours, images were captured using a 40x objective on a Nikon Eclipse Ti2 microscope. Images of a 10 μm divisions calibration slide (#MA663, Swift Microscope World, Carlsbad, CA) were used for size bars. Three fields of view were chosen randomly for imaging. Image quantification was done using Image J (NIH, Bethesda, MD). Using the Set Scale function from Image J on a 1 mm scale bar image, all the images were calibrated to the same scale by applying the settings globally. Using the 'Straight' command, the length of the alveolar wall on the image was measured and was recorded with the 'Measure' command. Eight measurements of the alveolar wall thickness were recorded for each image.

To assess exudates in the alveoli, for each mouse, for the stained cryosections described above, three randomly chosen fields of view were photographed with a 20x objective, and both the number of exudate-containing alveoli and exudate-free alveoli in each image were counted. The percent of exudate-containing alveoli was then calculated. Using the Threshold function and the Measure Tool in NIH ImageJ, the percent area of each 20x objective image of lung cryosections described above containing tissue (not counting pale pink exudates) was measured, and this percentage was subtracted from 100% to obtain the percent area of the image occupied by the alveolar airspace. The threshold was then adjusted to obtain the percent area of the image occupied by tissue and exudate. The percent area of the image occupied by exudate was then calculated by subtracting the percent area of the image occupied by tissue from the percent area of the image occupied by tissue and exudate. The percentage of the exudate-occupied airspace area was then calculated by taking the ratio of (percent area of the image occupied by exudate)/(percent area of the image occupied by the alveolar airspace), and converting the fraction to a percentage.

Lung sections were also assessed for the presence of immune cells using anti-CD11b, anti-CD11c, anti-CD45, anti-Ly6G, or anti-Mac2 (clone M3/38; BioLegend) antibodies with isotype-matched irrelevant rat antibodies (400501, clone RTK2758 and 400602, clone RTK4530, BioLegend) as controls. Lung sections were first incubated with PBS containing 4% BSA (PBS-BSA) for 60 minutes to block non-specific binding, and the endogenous biotin was blocked by the addition of streptavidin and biotin solutions, following the manufacturers' instructions (Streptavidin/Biotin Blocking Kit, Vector Laboratories, Burlingame, CA). Sections

were then stained as described above. Positively stained cells were counted from randomly selected fields, and presented as the number of positive cells per mm^2.

Cell isolation and culture

Human peripheral blood was collected from healthy volunteers who gave written consent and with specific approval from the Texas A&M University human subjects review board. All the methods were performed in accordance with the relevant guidelines and regulations. Peripheral blood mononuclear cells (PBMCs) were isolated and collected from blood using Ficoll-Paque density gradient centrifugation (GE Healthcare, Cincinnati, OH) following the manufacturer's protocol. PBMCs were cultured at 10^4 cells/well in a total volume of 200 μL/well in 96-well flat bottom tissue culture plates (#353072; Falcon-Corning, Corning, NY) in RPMI-1640 (Lonza, Walkersville, MD) supplemented with 10 mM HEPES (Lonza)), 1× nonessential amino acids (Lonza), 1 mM sodium pyruvate (Lonza), 2 mM glutamine (Lonza), 100 U/mL penicillin, 100 μg/mL streptomycin (Lonza), 1× ITS-3 (Sigma-Aldrich, St. Louis, MO), and 10 ng/ml of macrophage-colony stimulating factor (M-CSF, BioLegend). The cells were then incubated at 37˚C with 5% CO_2. After 120 hours, 100 microlitres of the medium from the PBMCs were removed and replaced with medium in the presence or absence of ORN06 to a final concentration of 0–1 μg/mL. and 1 μg/mL of recombinant human SAP. The ORN06 and recombinant human SAP was diluted in RPMI-medium and added to cells to make the total volume of 200 μL in a well. The culture media supernatants were collected after 48 h and assayed using interleukin-6 (IL-6) ELISA kits (Biolegend) following the manufacturer's protocols, reading absorbance with a SynergyMX plate reader (BioTek, Winooski, VT).

BALF and serum cytokines and D-dimer assays

BALF was collected as described previously [34,51]. After mice were euthanized, blood was collected from the abdominal aorta and chilled on ice. After 30 minutes, the blood was clarified by centrifugation at 10,000 × g for 5 minutes at 4˚C to isolate serum, which was then stored at -80˚C [56–58]. Sera were assayed for cytokines using a 13-plex LEGENDplex Mouse Inflammation Panel kit (Biolegend, San Diego, CA) following the manufacturer's instructions using an Accuri C6 flow cytometer (BD Bioscience, Franklin Lakes, NJ). D-dimer levels were assayed using a mouse D-dimer kit (#MBS764560, MyBioSource, San Diego, CA) following the manufacturer's instructions.

Statistics

Statistical analyses with t tests or 1-way ANOVA with the indicated post-test were done using GraphPad Prism 7 (GraphPad, San Diego, CA). Significance was defined as $p < 0.05$. Using G*Power analysis [59,60] and previous historical data, a total sample of size of at-least 3 mice per group was determined to be sufficient to detect effect sizes anticipated in the present experiments. Post euthanasia, the lungs harvested from one control female mouse were not properly inflated with the Surgipath frozen section compound. Two additional female mice were used in the control group for statistical analysis.

Results

Aspirated ORN06 increases cells in mouse BALF, and SAP injections counteract this

To determine if aspiration of ORN06 can induce lung inflammation and damage, and whether SAP injections might affect this, mice were treated with an oropharyngeal aspiration of

ORN06, and then at 24 and 48 hours, mice were treated with intraperitoneal injections of SAP or buffer. Mice were then euthanized at 72 hours. Compared to control (PBS aspirated and then PBS injected), for male and female mice, ORN06 (1 mg/ kg ORN06 aspirated and then PBS injected) caused a large increase in the number of cells recovered from the BALF, and SAP ameliorated the ORN06-induced increase (Fig 1A and S2A Fig). Preliminary experiments with 0.01 and 0.1 mg/ kg ORN06 showed 2.5 x 10^4 and 3.3 x 10^4 cells respectively in the BALF for 1 male mouse at each dose. Assessing cell type by Wright-Giemsa staining, for male and female mice, compared to control, ORN06 increased the number of monocyte/macrophages, and SAP treatments reversed these ORN06-induced increases (Fig 1B and S2B Fig). Similar results were observed for lymphocytes, with the exception that control males had more BALF

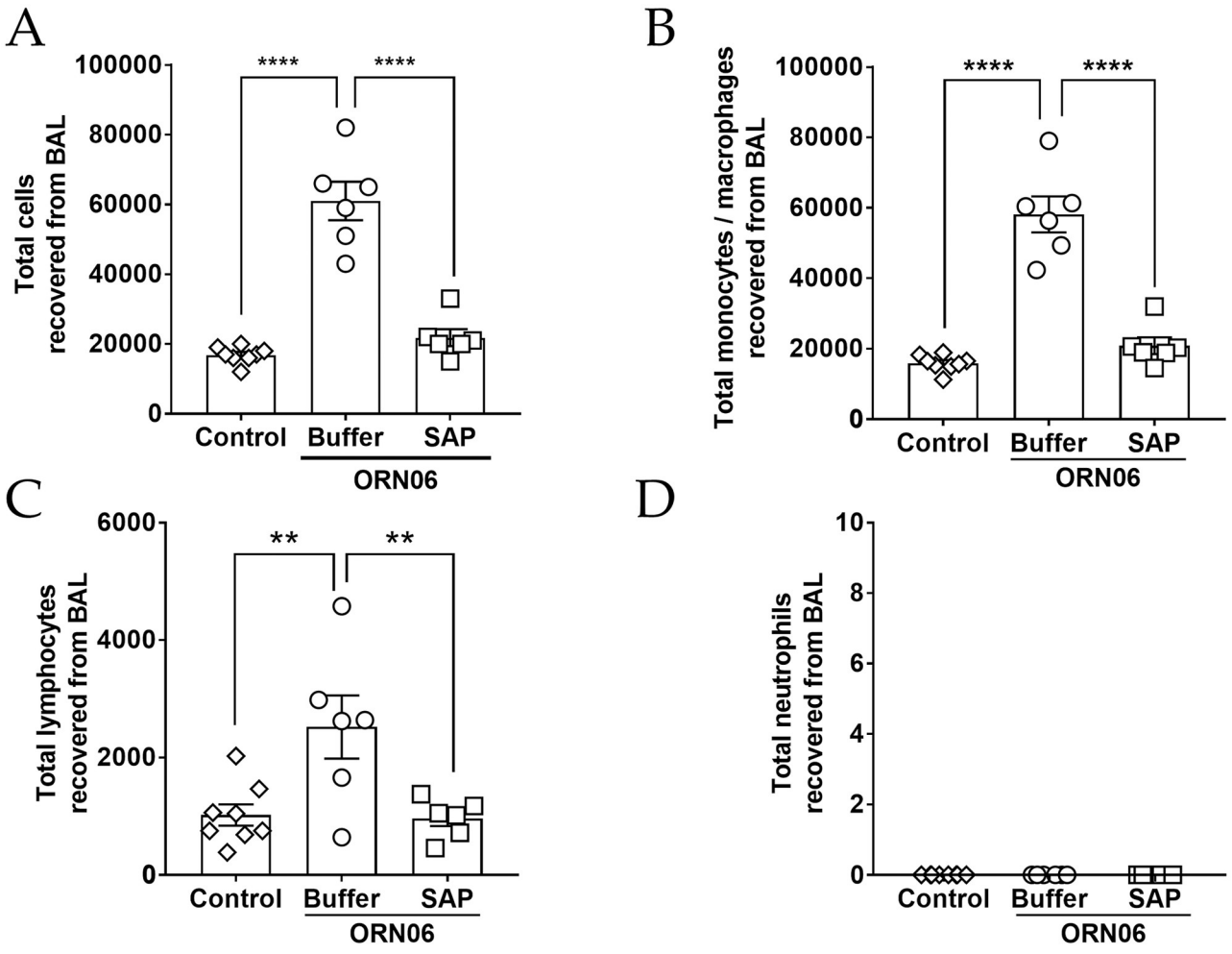

Fig 1. SAP attenuates ORN06-induced upregulation of total cells and immune cell types in mouse BAL. (A) The total number of cells collected from the BALF at day 3 post ORN06 aspiration. Cell spots of BALF at day 3 post ORN06 aspiration were stained with Wright-Giemsa stain. **(B)** The percentages of monocytes/macrophages were determined by examining at least 150 cells per mouse BAL sample. Values are mean ± SEM, n = 6 mice (3 males and 3 females), except control group where n = 8 (3 males and 5 females). ** $p < 0.01$ and **** $p < 0.0001$ (1-way ANOVA, Bonferroni's test). There was no significant difference between the control group and the SAP-treated group. **(C)** The percentages of lymphocytes were determined by examining at least 150 cells per mouse BAL sample. Values are mean ± SEM, n = 6 mice (3 males and 3 females), except control group where n = 8 (3 males and 5 females). ** $p < 0.01$ and **** $p < 0.0001$ (1-way ANOVA, Bonferroni's test). There was no significant difference between the control group and the SAP-treated group. **(D)** The percentages of neutrophils were determined by examining at least 150 cells per mouse BAL sample. Values are mean ± SEM, n = 6 mice (3 males and 3 females), except control group where n = 8 (3 males and 5 females). ** $p < 0.01$ and **** $p < 0.0001$ (1-way ANOVA, Bonferroni's test). there was no significant difference between the control group and the SAP-treated group.

https://doi.org/10.1371/journal.pone.0245924.g001

lymphocytes that control females, and the ORN06 treated males showed a wide range of BALF lymphocyte counts and this was thus not statistically different from control (Fig 1C and S2C Fig). The ORN06 treatment did not significantly increase the number of neutrophils in the BALF from male or female mice (Fig 1D and S2D Fig). Compared to ORN06 alone, SAP injections in ORN06-treated mice increased body weight at day 3, with a significant effect in female but not male mice (S3 Fig). For male and female mice, the ORN06 treatment with or without SAP caused no significant difference in liver, heart, kidneys, spleen, white fat, or brown fat weights as a percentage of body weight at day 3 (S4 Fig).

Immunohistochemistry on BALF cell spots indicated that compared to control, ORN06 increased the number of CD11c-positive macrophages and/or dendritic cells, and increased the number of CD45-positive leukocytes for both male and female mice, and these effects were reversed with SAP injections (Fig 2, S5C and S5D Fig). Male control mice had more CD11b-positive blood and inflammatory macrophages in the BALF than female control mice (S5B Fig). Compared to control, ORN06 increased the number of CD11b positive cells in the BALF from female mice but not male mice, and SAP treatments reversed the ORN06-induced increase in the female mice (S5B Fig). The ORN06 treatment did not significantly increase the number of CD3-positive lymphocytes or Ly6G-positive neutrophils in the BALF from male or female mice (Fig 2, S5A and S5E Fig). Together, these results indicate that inhaled ORN06 causes an increase in monocytes/macrophages and CD-3 negative lymphocytes in the lung airspace, and that SAP injections can reverse this.

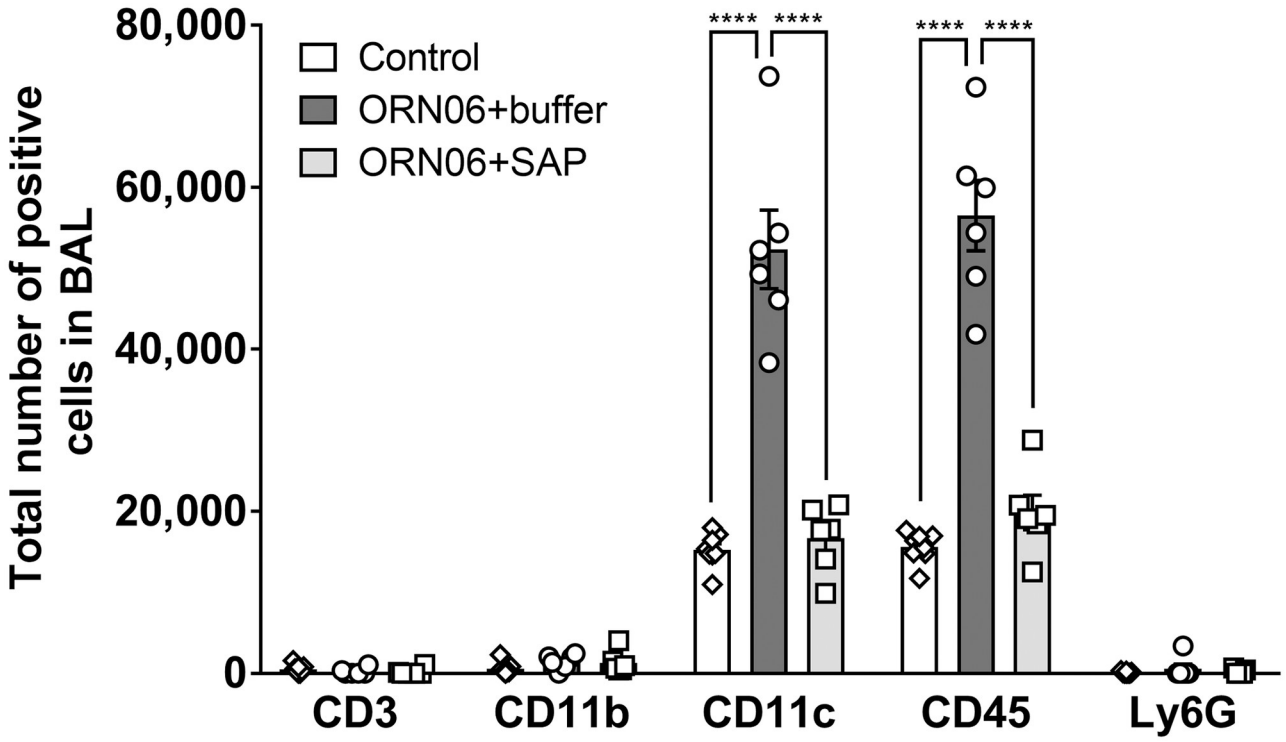

Fig 2. SAP attenuates ORN06-induced upregulation of inflammatory cells in mouse BAL. Cell spots of BALF at day 3 were stained for the indicated markers. The percentage of cells stained was determined in 5 randomly chosen fields of 100–150 cells, and the percentage was multiplied by the total number of BALF cells for that mouse to obtain the total number of BALF cells staining for the marker. Values are mean ± SEM, n = 6 mice (3 males and 3 females), except control group where n = 8 (3 males and 5 females). **** $p < 0.001$ (1-way ANOVA, Dunnett's test). There was no significant difference between the control group and the SAP-treated group.

https://doi.org/10.1371/journal.pone.0245924.g002

Aspirated ORN06 increases the local density of macrophages remaining in mouse lungs after BAL, and SAP injections counteract this

After BAL, lungs were inflated and cryosections were immunostained to determine if ORN06 aspiration affects the local density of selected immune cells. Compared to control, ORN06 increased the density of CD11b positive blood and inflammatory macrophages and CD45 positive leukocytes, and SAP reversed this, for male and female mice (Fig 3, S6 and S7 Figs). The ORN06 treatment with or without SAP caused a greater local density of CD11b positive cells in male compared to female mice, and ORN06 alone caused a greater number of CD45 positive cells in male mice (S7 Fig). Compared to control, ORN06 increased the density of CD11c positive alveolar macrophages and dendritic cells, and SAP reversed this, with significant effects for female but not male mice (Fig 3 and S7B Fig). ORN06 with or without SAP had no significant effect for male or female mice on the local density of Mac2/Gal3 positive alveolar macrophages [61] or Ly6G positive neutrophils (Fig 3, S7C and S7E Fig).

Aspirated ORN06 increases clot-like aggregates in male mouse BALF, and SAP injections may counteract this and attenuates D-dimer levels in BALF

We noticed that the ORN06 treatment with subsequent buffer injections caused the formation of irregular clot-like aggregates visible as dark blue irregular objects in the Wright-Giemsa-stained BALF from 2 of 3 male mice (Fig 4A). Defining a clot-like aggregate as an irregularly shaped 2–10 μm object in the BALF staining dark blue with Wright-Giemsa stain, no clot-like aggregates were observed in the BALF cell spots from the 3 male and 5 female control mice or

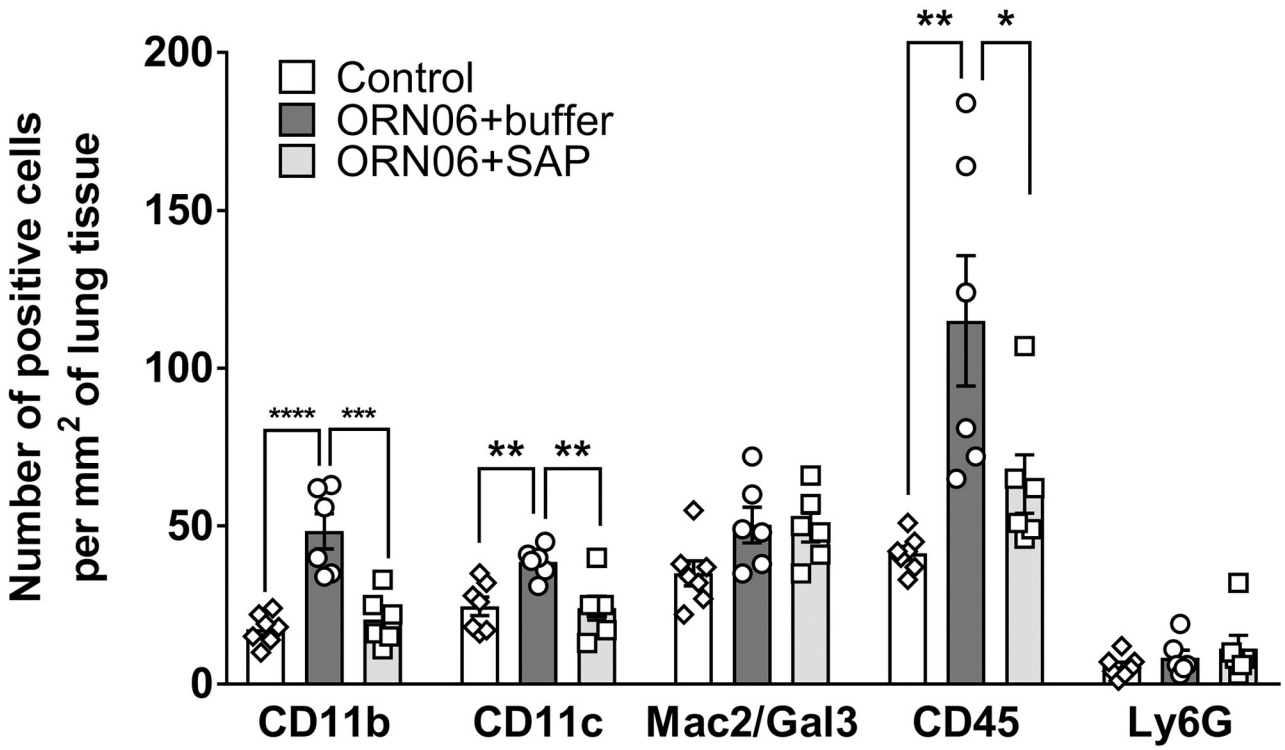

Fig 3. SAP attenuates ORN06-induced upregulation of inflammatory cells in lung tissues post-BAL. Day 3 lung cryosections were stained for the indicated markers. The number of cells stained was determined in 6 randomly chosen 450 μm diameter fields, and the number of positive cells per mm^2 of lung tissue was calculated for each marker. Values are mean ± SEM, n = 6 mice (3 males and 3 females), except control group where n = 7 (3 males and 4 females). * $p < 0.05$, ** $p < 0.01$, *** $p < 0.001$, and **** $p < 0.0001$ (1-way ANOVA, Dunnett's test).

https://doi.org/10.1371/journal.pone.0245924.g003

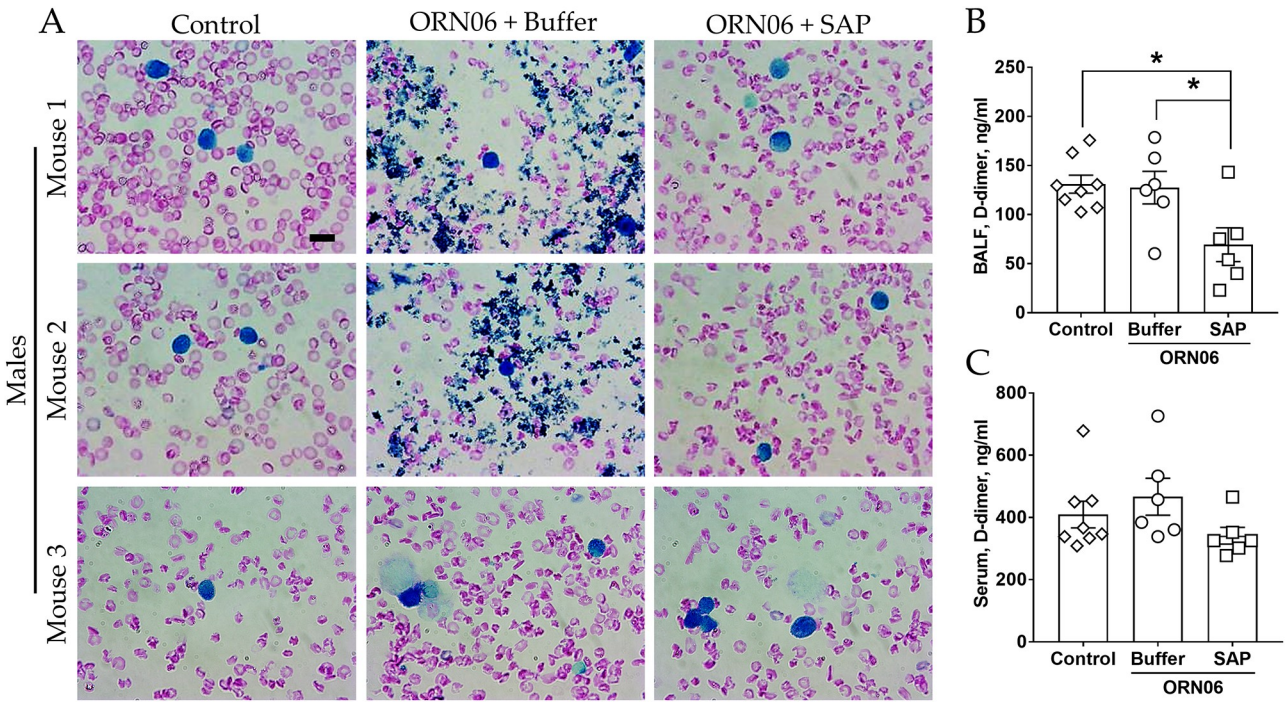

Fig 4. SAP attenuates ORN06-induced clot formation in mouse BAL. (A) Cell spots of BALF at day 3 were stained with Wright-Giemsa stain. The left two images are of BALF cell spots from three different control male mice. The middle two images are of BALF cell spots from three different male mice treated with buffer after ORN06 insult he right two images are of BALF cell spots from three different male mice treated with SAP after ORN06 insult. Bar is 10 μm. Quantification of d-dimer levels detected in mouse (**B**) BALF and (**C**) serum for control, ORN06 and then buffer, and ORN06 and then SAP-treated mice. Values are mean ± SEM, n = 6 mice (3 males and 3 females), except control group where n = 8 (3 males and 5 females). * $p < 0.05$ (1-way ANOVA, Bonferroni's test).

https://doi.org/10.1371/journal.pone.0245924.g004

the 3 male and 3 female ORN06-treated with subsequent SAP injections mice. These results indicate that SAP injections may inhibit the formation of clot-like aggregates in the lungs.

D-dimers are the degradation products of fibrin, a major component of blood clots [62]. D-dimers levels are widely used to determine the severity of diseases such as COVID-19 [63,64]. Compared to the control group, for male and female mice, ORN06 aspirated and buffer-injected mice showed no significant difference in the BALF D-dimers levels, and ORN06 aspirated and SAP-injected mice showed reduced BALF D-dimers levels (Fig 4B and S8 Fig). There were no significant changes in the serum D-dimers levels between any groups (Fig 4C and S8 Fig). These results indicate SAP injections may inhibit the formation of fibrin clots in the lungs.

Aspirated ORN06 increases alveolar wall thickness and exudates in the alveoli in mice, and SAP injections can counteract this

Compared to the control group, for male and female mice, ORN06 aspirated and buffer-injected mice showed an increase in alveolar wall thickness, and this was reduced by treatment with SAP (Fig 5A–5D and S9A Fig). ORN06 treatment with or without SAP caused a larger increase on alveolar wall thickness in female compared to male mice (S9 Fig). We also noticed that for male and female mice, ORN06 caused the formation of exudates visible as light pink objects in the interior of alveoli (the alveolar airspace) in cryosections stained with hematoxylin & eosin (red arrow, Fig 5B, 5E and 5F and S9 Fig). This effect was reversed by SAP injections (Fig 5A–5C, 5E and 5F and S9 Fig). Compared to female mice, male mice

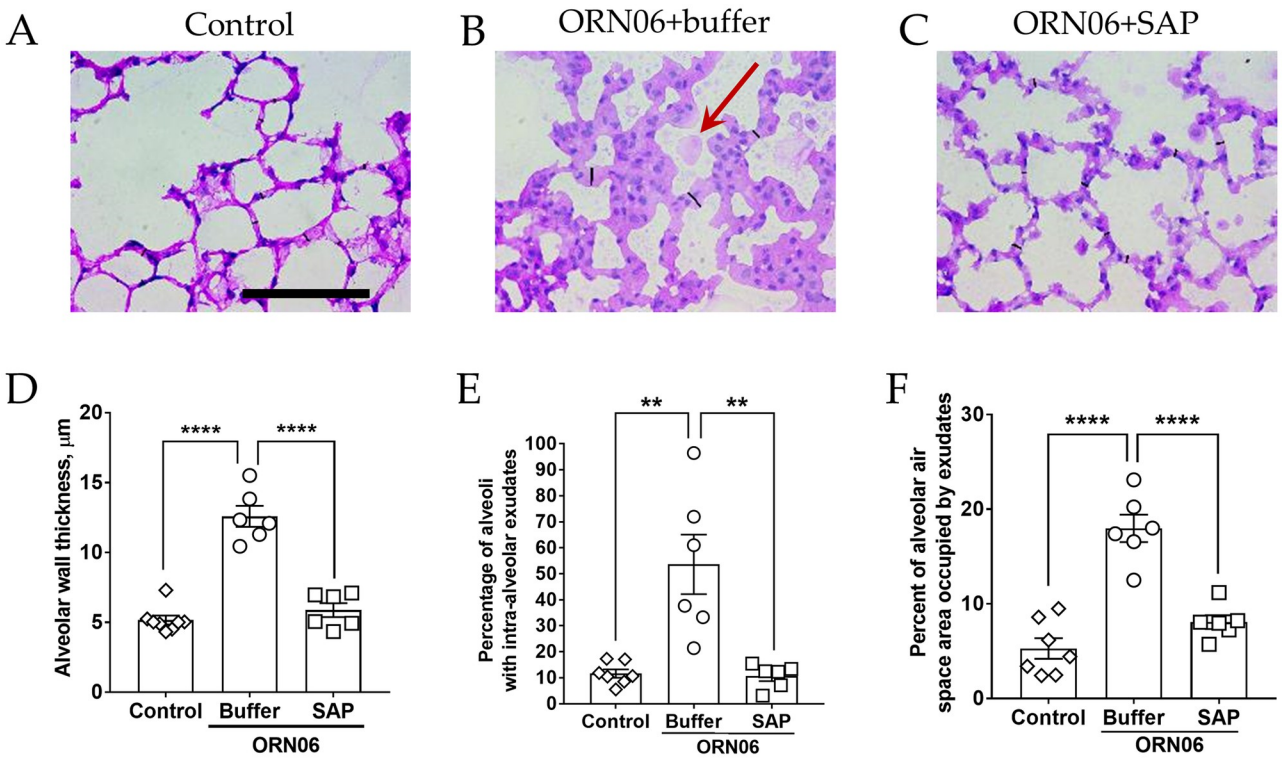

Fig 5. SAP attenuates ORN06-induced alveolar wall thickness. Day 3 lung cryosections of **(A)** control, **(B)** ORN06+buffer, and **(C)** ORN06+SAP were stained with H&E. Images are representative of mice from each group. The thin black lines on the images are the representation of the measured alveolar wall thickness. Scale bar (thick black bar) is 100 μm. Red arrow indicates an exudate in the alveolar air space. **(D)** Quantification of alveolar wall thickness in lung cryosections. Values are mean ± SEM, n = 6 mice (3 males and 3 females) except the control group where n = 8 (3 males and 5 females). ** $p < 0.01$ and **** $p < 0.0001$ (1-way ANOVA, Bonferroni's test). **(E)** Quantification of the percentage of alveoli containing one or more exudates in the alveolar airspace observed in lung-section micrographs. Values are mean ± SEM, n = 6 mice (3 males and 3 females) except the control group where n = 7 (3 males and 4 females). ** $p < 0.01$ and **** $p < 0.0001$ (1-way ANOVA, Bonferroni's test). **(F)** Quantification of the percentage area of alveoli airspace containing exudate observed in micrographs of lung sections. Values are mean ± SEM, n = 6 mice (3 males and 3 females) except the control group where n = 7 (3 males and 4 females). ** $p < 0.01$ and **** $p < 0.0001$ (1-way ANOVA, Bonferroni's test).

https://doi.org/10.1371/journal.pone.0245924.g005

had a greater percentage of alveoli containing ORN06-induced exudates (S9 Fig). Together, these results indicate that ORN06 inhalation increases alveolar wall thickness and the formation of exudates in alveoli, and that SAP injections can inhibit both of these ORN06-induced effects.

Aspirated ORN06 increases some serum cytokines in mice, and SAP injections can counteract this

Compared to control, ORN06 treatment of mice caused serum concentrations of IL-1β, IL-6, IL-12p70, IL-23, and IL-27 to increase at day 3, and SAP injections decreased all of these ORN06-induced increases (Fig 6A–6E). Male mice had a somewhat greater ORN06-induced increase in IL-6 than female mice, but did not show an ORN06-induced increase in IL-23 (S10 Fig). ORN06 decreased IL-17 levels, and had no significant effect on levels of several other cytokines, while SAP increased IL-10 and restored IL-17A in ORN06-treated female mice, and decreased MCP-1 in ORN06-treated male mice (S11 and S12 Figs). Together, these results suggest that ORN06 inhalation increases some serum cytokines in mice, and that SAP injections can inhibit these ORN06-induced effects.

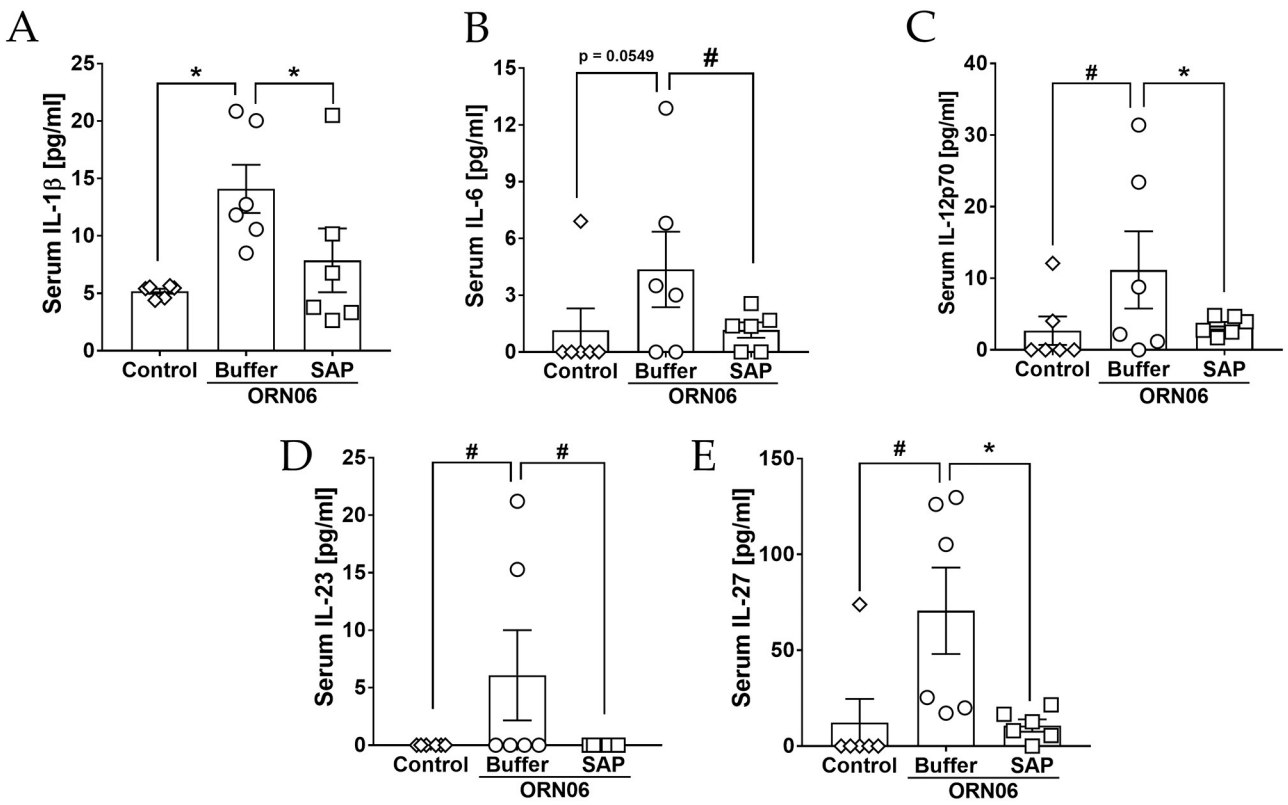

Fig 6. SAP attenuates ORN06-increased serum cytokine levels. Quantification of **(A)** IL-1β, **(B)** IL-6, **(C)** IL-12p70, **(D)** IL-23, and **(E)** IL-27 levels detected in mouse serum for control, ORN06 and then buffer, and ORN06 and then SAP-treated mice. Values are mean ± SEM, n = 6 mice (3 males and 3 females). * $p < 0.05$ and ** $p < 0.01$ (t-test). # $p < 0.05$ (Welch's t-test).

https://doi.org/10.1371/journal.pone.0245924.g006

ORN06 treatment upregulates extracellular accumulation of IL-6 from human PBMC and SAP treatment attenuates this

To determine if ORN06 might cause human cells to accumulate extracellular IL-6, human PBMC were cultured in the presence of 10 ng/ml of M-CSF and in the absence or presence of ORN06. The extracellular accumulation of IL-6 was upregulated by 1 μg/mL of ORN06 treatment (Fig 7A). Compared to control, 1 μg/mL of ORN06 treatment caused extracellular accumulation of IL-6 after 48 hours, and SAP decreased the ORN06-induced increase of IL-6 (Fig 7B). Similar to mice, human PBMC from males but not females had an ORN06-induced increase in IL-6 (S13 Fig). Together, these results suggest that in human cells, ORN06 treatment increases the proinflammatory cytokine IL-6, and that SAP can inhibit this.

Discussion

In this report, we observed that aspiration of ORN06 induced the accumulation of immune cells, alveolar wall thickening, and presence of lung exudates, as previously described when mice were treated with GU-rich ssRNA by tail vein injection [47]. Aspiration of ORN06 also led to the formation of clot-like aggregates in some male mouse lung fluids. ORN06 aspiration increased levels of CD11b+, CD11c+, and CD45+ macrophages, CD3- lymphocytes, but not Ly6G positive neutrophils in the lungs, and upregulated IL-1β, IL-6, IL-12p70, IL-23, and IL-27 in the serum and extracellular IL-6 accumulation from human PBMC. We also observed

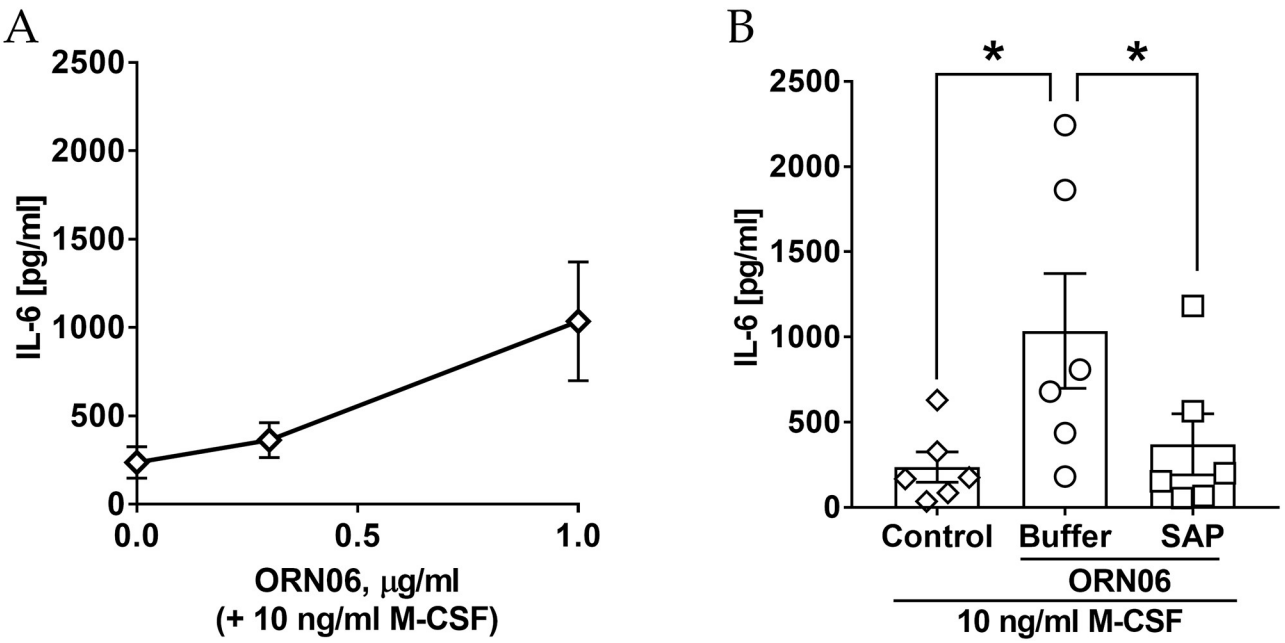

Fig 7. SAP attenuates ORN06-increased extracellular IL-6 from human PBMC. (A) Quantification of extracellular IL-6 accumulation post ORN06 treatment at 0–1 μg/mL and 10 ng/ml M-CSF. **(B)** Quantification of extracellular IL-6 levels for control, ORN06 and then buffer, and ORN06 and then SAP-treated human PBMC cultured in presence of 10 ng/ml M-CSF. Values are mean ± SEM, n = 6 (human PBMC from 3 males and 3 females). * $p < 0.05$ (1-way ANOVA, Bonferroni's test).

https://doi.org/10.1371/journal.pone.0245924.g007

differences in the response to ORN06 between male and female mice. Unlike tail vein injection, aspiration of the GU-rich ssRNA did not induce death of the mice over 72 hours [47]. In mice treated with aspirated ORN06, injections of SAP attenuated lung inflammation, alveolar wall thickening, the presence of lung exudates and clot-like aggregates, and elevated serum cytokines induced by ORN06 aspiration. Although ORN06 did not increase D-dimer levels at 3 days (clot breakdown may occur at later times), SAP decreased D-dimer levels in lung fluid. SAP also attenuated ORN06-induced upregulation of IL-6 from human PBMC. These results suggest that ORN06 aspiration mimics some of the characteristics of COVID-19, and that SAP could be a potential therapeutic for severe COVID-19 disease and other conditions where a cytokine storm is a clinical problem.

Compared to both healthy controls and patients with viral or bacterial pneumonia, COVID-19 patients, especially severe cases, have in their peripheral blood reduced numbers of CD14+CD16-DR+ "classical" monocytes, which may be due to the increased levels of IL-6 and/or dysregulated myelopoiesis [1,4,65–68]. In the BAL, patients with severe COVID-19 have more macrophages than mild cases or healthy controls, and the increased macrophage numbers appear to be due to the presence of recruited monocyte-derived inflammatory macrophages [1,15,16,69]. We found that ORN06-induced increases in BALF cell counts were mirrored by an increase in CD11c+ and CD45+ cells with the morphology of macrophages, suggesting that ORN06 stimulates the accumulation of CD11c+CD45+ alveolar macrophages, but whether this is due to the proliferation of resident alveolar macrophages, migration of CD11c+CD45+ interstitial macrophages into the alveoli, or a rapid phenotypic conversion of recruited CD11b+CD11c- to CD11b-CD11c+ macrophages is unknown [70,71]. Aspiration of ORN06 led to increased numbers of CD11b+, CD11c+, and CD45 + cells, but not Mac2/Gal3 positive cells, retained in the lungs after BAL. As Mac2/Gal3 is a marker for tissue resident lung macrophages [61], these data suggest that ORN06 generates

a response that induces the recruitment of CD11b+CD45+ inflammatory macrophages, which may undergo phenotypic conversion to CD11b-CD11c+CD45+ macrophages, and/or ORN06 induces the proliferation of lung resident CD11c+CD45+ interstitial macrophages [35,70,71]. Injections of SAP attenuated the accumulation of macrophages in both the BAL fluid and in the post-BAL lung tissue. These data suggest that SAP can be used to target the recruited macrophage populations without altering the tissue resident macrophages, or elevating the neutrophils in the lung.

We use human SAP in the mouse model. The UniProt sequences P02743 for human SAP and P12246 for murine SAP show 69.1% identity and 87.9% similarity [72]. In vitro, human and mouse SAP both inhibit human and mouse immune cell differentiation, with approximately similar efficacy [23,73]. Several studies have also reported that human and murine SAP have the same efficacy to inhibit inflammation and fibrosis in multiple mouse models [27,28,30,31,41,74,75].

ORN06 aspiration also led to a small but significant increase in the number of BALF lymphocytes, which were CD3 negative, suggesting this was due to either the recruitment of CD3 negative natural killer (NK) cells or other types of innate lymphoid cells (ILC), or the proliferation of lung resident ILCs [76–78]. SAP was also effective at attenuating the ORN06-induced increase in BALF lymphocytes.

COVID-19 patients have reduced numbers of ILC, including NK cells, in the peripheral blood, but scRNA-seq analysis from COVID-19 patients indicate higher numbers of NK cells in the BAL [67]. NK cells and other ILCs are potent producers of a variety of cytokines, depending on the subtype of ILCs, stimulus, and tissue where the ILCs are found, but how the changes in the number and composition of ILCs subsets affect cytokine levels in COVID-19 is still unclear [1,79]. COVID-19 is also characterized by a "cytokine storm" with increased levels of pro-inflammatory cytokines in the blood, such as IL-1β, TNF-α, IL-6, IL-12 [4,67,68,80], and we detected increased IL-1β, IL-6, IL-12, IL-23, and IL-27 in the serum following ORN06 aspiration. Injections of SAP attenuated the increased levels of the above cytokines, suggesting that SAP can either induce cells to degrade extracellular cytokines, or inhibit cells from secreting cytokines the above cytokines. SAP also elevated the serum levels of the "anti-inflammatory cytokine" IL-10, as observed previously [25,32,37]. Previous studies suggest that IL-17A plays an important role in enhancing antiviral T helper type 1 responses in the female genital tract, where female mice lacking IL-17A have lower proportions of IFN-γ+ T_h1 cells than wild type female mice [81]. Compared to male mice, female mouse bladders have higher IL-17 expression [82]. We observed that ORN06 decreased serum IL-17A in female but not male mice, and that SAP reversed the ORN06 effect in female mice. Together, this suggests that SAP can reverse the effects of ORN06 on several serum cytokines.

Severe COVID-19 disease is 1.5 to 2 times higher in men than women [4–7]. We found that ORN06 aspiration led to a higher BALF cell numbers, clot-like aggregates, and alveoli containing exudates in male mice compared to female mice, which suggests a similar response in mice compared to humans. Many diseases are associated with sex-based differences in disease incidence, prevalence, and severity [83–85], but the causes of these differences for COVID-19 in particular remain unclear.

Together, our results and the work described above suggest the intriguing possibility that aspiration of oligonucleotides such as ORN06 could be a simple model for ssRNA virus infections like SARS-CoV-2. In addition, SAP strongly attenuated the effects of aspiration of ORN06, suggesting that SAP could be a potential therapeutic for severe ssRNA virus diseases and possibly other diseases where a cytokine storm is a contributing factor for disease severity or progression.

Supporting information

S1 Fig. Coomassie blue stained gel of purified recombinant human SAP. As described in the materials and methods section, the purified human SAP showed a single band at the expected molecular mass of ~26 kiloDaltons (kDa). Lane A is protein molecular mass marker with masses indicted in kDa. Lanes B and C are purified recombinant human SAP.
(TIF)

S2 Fig. Cells in male and female mouse BAL. (A) The data from Fig 1A–1D were separated for male (M) and female (F) mice from each group for **(A)** total cells, **(B)** monocytes/macrophages, **(C)** lymphocytes, and **(D)** neutrophils. Values are mean ± SEM. For male mice n = 3 in each group and for female mice n = 3 except for female mice control group, where n = 5. ** $p < 0.01$ and *** $p < 0.001$ (1-way ANOVA, Bonferroni's test). # $p < 0.05$ (t-test).
(TIF)

S3 Fig. SAP treated mice are resistant to a decline in body weight after ORN06 aspiration. Percent change in body weight for **(A)** both males and females, **(B)** males, and **(C)** females after the indicated treatments. Values are mean ± SEM, n = 6 (3 males and 3 females) except for PBS-aspirated and then PBS-treated, where n = 8 (3 males and 5 females). * $p < 0.05$ and ** $p < 0.01$ (1-way ANOVA, Bonferroni's test).
(TIF)

S4 Fig. Organ weights. Organ weights as percent of total body weight at day 3 of **(A)** both male and female mice, **(B)** males, and **(C)** females after the indicated treatments. Values are mean ± SEM, n = 6 (3 males and 3 females) except for control, where n = 8 (3 males and 5 females).
(TIF)

S5 Fig. Specific cell types in male and female mouse BAL. The data from Fig 2 was separated for **(A)** CD3 positively stained cells, **(B)** CD11b positively stained cells, **(C)** CD11c positively stained cells, **(D)** CD45 positively stained cells, and **(E)** Ly6G positively stained cells from male (M) and female (F) mice from each group. Values are mean ± SEM. For male mice n = 3 and for female mice n = 3 except for female mice control group, where n = 5. ** $p < 0.01$, *** $p < 0.001$, and **** $p < 0.0001$ (1-way ANOVA, Bonferroni's test). # $p < 0.05$ (t-test).
(TIF)

S6 Fig. Images of stained post-BAL lung cryosections. Representative images of male and female mouse lung cryosections stained with antibodies against CD45 and CD11b. Red is staining, blue is counter stain. Bar is 100 μm. Images are representative of n = 3 in each male and female group, except for female mouse control group, where n = 4.
(TIF)

S7 Fig. Specific cell types in male and female mouse post-BAL lung cryosections. The data from Fig 3 was separated for **(A)** CD11b positively stained cells, **(B)** CD11c positively stained cells, **(C)** Mac2/Gal3 positively stained cells, **(D)** CD45 positively stained cells, and **(E)** Ly6G positively stained cells from male (M) and female (F) mice from each group. Values are mean ± SEM. For male mice n = 3 and for female mice n = 3 except for female mice control group, where n = 4. * $p < 0.05$, ** $p < 0.01$, and *** $p < 0.001$ (1-way ANOVA, Dunnett's test). # $p < 0.05$ and ## $p < 0.01$ (t-test).
(TIF)

S8 Fig. D-dimers levels from male and female mouse BALF and serum. The data from Fig 4B and 4C were separated for **(A)** BALF and **(B)** Serum D-dimers levels from male (M) and female (F) mice from each group.
(TIF)

S9 Fig. Alveolar wall thickness and alveolar exudates in in male and female mice. The data from Fig 5D, 5E and 5F were separated for **(A)** alveolar wall thickness, **(B)** percent of alveoli with intra-alveolar exudates, and **(C)** percent of alveolar airspace area occupied by exudates from male (M) and female (F) mice from each group. Values are mean ± SEM. For male mice n = 3 in each group and for female mice n = 3 except for female mice control group in (A), where n = 5 and in (B–C), where n = 4. * $p < 0.05$, ** $p < 0.01$, *** $p < 0.001$, and **** $p < 0.0001$ (1-way ANOVA, Bonferroni's test). # $p < 0.05$, ### $p < .001$ (t-test).
(TIF)

S10 Fig. Cytokine levels from male and female mouse sera. The data from Fig 6A, 6B, 6C, 6D and 6E were separated for serum **(A)** IL-1β, **(B)** IL-6 **(C)** IL-12p70, **(D)** IL-23, and **(E)** IL-27 levels from male (M) and female (F) mice from each group. Values are mean ± SEM. For male mice and female mice n = 3 in each group. * $p < 0.05$ and *** $p < 0.001$ (t-test).
(TIFF)

S11 Fig. Cytokine levels from mouse sera. Sera were collected at day 3 and assayed by ELISA for the indicated cytokines. Values are mean ± SEM, n = 6 (3 males and 3 females). * $p < 0.05$ (1-way ANOVA, Bonferroni's test).
(TIFF)

S12 Fig. Cytokine levels from male and female mice sera. The data from S11 Fig were separated for serum **(A)** IL-1α, **(B)** IL-10 **(C)** IL-17, **(D)** GM-CSF, **(E)** IFN-γ, **(F)** IFN-β, **(G)** MCP-1, and **(H)** TNF-α levels from male (M) and female (F) mice from each group. Values are mean ± SEM. For male mice and female mice n = 3 in each group. * $p < 0.05$ and ** $p < 0.01$ (t-test).
(TIFF)

S13 Fig. Extracellular IL-6 levels from human males and female PBMCs. The data from Fig 7A and 7B were separated for males (M) and females (F). Values are mean ± SEM, n = 3 for each group. * $p < 0.05$ (1-way ANOVA, Bonferroni's test).
(TIFF)

S1 Data.
(XLSX)

Author Contributions

Conceptualization: Tejas R. Karhadkar, Darrell Pilling, Richard H. Gomer.

Formal analysis: Tejas R. Karhadkar, Darrell Pilling, Richard H. Gomer.

Funding acquisition: Richard H. Gomer.

Investigation: Tejas R. Karhadkar, Darrell Pilling.

Methodology: Tejas R. Karhadkar, Darrell Pilling, Richard H. Gomer.

Writing – original draft: Tejas R. Karhadkar, Darrell Pilling, Richard H. Gomer.

Writing – review & editing: Tejas R. Karhadkar, Darrell Pilling, Richard H. Gomer.

References

1. Vabret N, Britton GJ, Gruber C, Hegde S, Kim J, Kuksin M, et al. Immunology of COVID-19: Current State of the Science. Immunity. 2020; 52(6):910–41. https://doi.org/10.1016/j.immuni.2020.05.002 PMID: 32505227
2. Crayne CB, Albeituni S, Nichols KE, Cron RQ. The Immunology of Macrophage Activation Syndrome. Frontiers in Immunology. 2019; 10(119). https://doi.org/10.3389/fimmu.2019.00119 PMID: 30774631
3. Schulert GS, Cron RQ. The genetics of macrophage activation syndrome. Genes & Immunity. 2020; 21 (3):169–81. https://doi.org/10.1038/s41435-020-0098-4 PMID: 32291394
4. Zhou X, Yang G, Guan F. Biological Functions and Analytical Strategies of Sialic Acids in Tumor. Cells. 2020; 9(2). Epub 2020/01/26. https://doi.org/10.3390/cells9020273 PMID: 31979120.
5. Gebhard C, Regitz-Zagrosek V, Neuhauser HK, Morgan R, Klein SL. Impact of sex and gender on COVID-19 outcomes in Europe. Biology of sex differences. 2020; 11(1):29-. https://doi.org/10.1186/s13293-020-00304-9 PMID: 32450906.
6. Scully EP, Haverfield J, Ursin RL, Tannenbaum C, Klein SL. Considering how biological sex impacts immune responses and COVID-19 outcomes. Nature Reviews Immunology. 2020; 20(7):442–7. https://doi.org/10.1038/s41577-020-0348-8 PMID: 32528136
7. Klein SL, Dhakal S, Ursin RL, Deshpande S, Sandberg K, Mauvais-Jarvis F. Biological sex impacts COVID-19 outcomes. PLoS pathogens. 2020; 16(6):e1008570–e. https://doi.org/10.1371/journal.ppat.1008570 PMID: 32569293.
8. Zhou F, Yu T, Du R, Fan G, Liu Y, Liu Z, et al. Clinical course and risk factors for mortality of adult inpatients with COVID-19 in Wuhan, China: a retrospective cohort study. Lancet (London, England). 2020; 395(10229):1054–62. Epub 2020/03/15. https://doi.org/10.1016/S0140-6736(20)30566-3 PMID: 32171076.
9. Tian S, Hu W, Niu L, Liu H, Xu H, Xiao SY. Pulmonary Pathology of Early-Phase 2019 Novel Coronavirus (COVID-19) Pneumonia in Two Patients With Lung Cancer. Journal of thoracic oncology: official publication of the International Association for the Study of Lung Cancer. 2020; 15(5):700–4. Epub 2020/03/03. https://doi.org/10.1016/j.jtho.2020.02.010 PMID: 32114094.
10. Barton LM, Duval EJ, Stroberg E, Ghosh S, Mukhopadhyay S. COVID-19 Autopsies, Oklahoma, USA. Am J Clin Pathol. 2020; 153(6):725–33. Epub 2020/04/11. https://doi.org/10.1093/ajcp/aqaa062 PMID: 32275742.
11. Wichmann D, Sperhake J-P, Lütgehetmann M, Steurer S, Edler C, Heinemann A, et al. Autopsy Findings and Venous Thromboembolism in Patients With COVID-19. Annals of Internal Medicine. 2020. https://doi.org/10.7326/M20-2003 PMID: 32374815
12. Beigmohammadi MT, Jahanbin B, Safaei M, Amoozadeh L, Khoshavi M, Mehrtash V, et al. Pathological Findings of Postmortem Biopsies From Lung, Heart, and Liver of 7 Deceased COVID-19 Patients. Int J Surg Pathol. 2020:1066896920935195. Epub 2020/06/20. https://doi.org/10.1177/1066896920935195 PMID: 32552178.
13. Fox SE, Akmatbekov A, Harbert JL, Li G, Brown JQ, Vander Heide RS. Pulmonary and Cardiac Pathology in Covid-19: The First Autopsy Series from New Orleans. medRxiv. 2020:2020.04.06.20050575. https://doi.org/10.1016/S2213-2600(20)30243-5 PMID: 32473124
14. Grobler C, Maphumulo SC, Grobbelaar LM, Bredenkamp JC, Laubscher GJ, Lourens PJ, et al. Covid-19: The Rollercoaster of Fibrin(Ogen), D-Dimer, Von Willebrand Factor, P-Selectin and Their Interactions with Endothelial Cells, Platelets and Erythrocytes. Int J Mol Sci. 2020; 21(14). Epub 2020/07/28. https://doi.org/10.3390/ijms21145168 PMID: 32708334.
15. Liao M, Liu Y, Yuan J, Wen Y, Xu G, Zhao J, et al. Single-cell landscape of bronchoalveolar immune cells in patients with COVID-19. Nature Medicine. 2020; 26(6):842–4. https://doi.org/10.1038/s41591-020-0901-9 PMID: 32398875
16. Bao L, Deng W, Huang B, Gao H, Liu J, Ren L, et al. The pathogenicity of SARS-CoV-2 in hACE2 transgenic mice. Nature. 2020; 583(7818):830–3. https://doi.org/10.1038/s41586-020-2312-y PMID: 32380511
17. Baltz ML, Dyck RF, Pepys MB. Amyloid P-component in mice injected with casein: identification in amyloid deposits and in the cytoplasm of hepatocytes. Immunology. 1980; 41(1):59–66. 8461. PMID: 7000694
18. Le PT, Mortensen RF. In vitro induction of hepatocyte synthesis of the acute phase reactant mouse serum amyloid P-component by macrophages and IL 1. JLeukocBiol. 1984; 35(6):587–603. 8140. https://doi.org/10.1002/jlb.35.6.587 PMID: 6610015
19. Pepys MB, Dyck RF, de Beer FC, Skinner M, Cohen AS. Binding of serum amyloid P-component (SAP) by amyloid fibrils. ClinExpImmunol. 1979; 38(2):284–93. 8471. PMID: 118839

20. Hamazaki H. Ca(2+)-dependent binding of human serum amyloid P component to Alzheimer's beta-amyloid peptide. J Biol Chem. 1995; 270(18):10392–4. Epub 1995/05/05. https://doi.org/10.1074/jbc.270.18.10392 PMID: 7737971.

21. Pepys MB, Booth DR, Hutchinson WL, Gallimore JR, Collins PM, Hohenester E. Amyloid P component. A critical review. Amyloid. 1997; 4:274–95. 8822.

22. Bharadwaj D, Mold C, Markham E, Du Clos TW. Serum amyloid P component binds to Fc gamma receptors and opsonizes particles for phagocytosis. JImmunol. 2001; 166(11):6735–41. 8055. https://doi.org/10.4049/jimmunol.166.11.6735 PMID: 11359830

23. Crawford JR, Pilling D, Gomer RH. FcγRI mediates serum amyloid P inhibition of fibrocyte differentiation. Journal of Leukocyte Biology. 2012; 92(4):699–711. https://doi.org/10.1189/jlb.0112033 PMID: 22493081

24. Cox N, Pilling D, Gomer RH. Distinct Fcγ receptors mediate the effect of Serum Amyloid P on neutrophil adhesion and fibrocyte differentiation. Journal of immunology (Baltimore, Md: 1950). 2014; 193(4):1701–8. https://doi.org/10.4049/jimmunol.1400281 PMID: 25024390.

25. Tam A, Churg A, Wright JL, Zhou S, Kirby M, Coxson HO, et al. Sex Differences in Airway Remodeling in a Mouse Model of Chronic Obstructive Pulmonary Disease. Am J Respir Crit Care Med. 2016; 193(8):825–34. Epub 2015/11/26. https://doi.org/10.1164/rccm.201503-0487OC PMID: 26599602.

26. Voltz JW, Card JW, Carey MA, Degraff LM, Ferguson CD, Flake GP, et al. Male sex hormones exacerbate lung function impairment after bleomycin-induced pulmonary fibrosis. American journal of respiratory cell and molecular biology. 2008; 39(1):45–52. Epub 2008/02/14. https://doi.org/10.1165/rcmb.2007-0340OC PMID: 18276795.

27. Haudek SB, Xia Y, Huebener P, Lee JM, Carlson S, Crawford JR, et al. Bone Marrow-derived Fibroblast Precursors Mediate Ischemic Cardiomyopathy in Mice. Proceedings of the National Academy of Sciences. 2006; 103(48):18284–9. 11371. https://doi.org/10.1073/pnas.0608799103 PMID: 17114286

28. Pilling D, Roife D, Wang M, Ronkainen SD, Crawford JR, Travis EL, et al. Reduction of bleomycin-induced pulmonary fibrosis by serum amyloid P. Journal of immunology (Baltimore, Md: 1950). 2007; 179(6):4035–44. Epub 2007/09/06. https://doi.org/10.4049/jimmunol.179.6.4035 PMID: 17785842.

29. Haudek SB, Trial J, Xia Y, Gupta D, Pilling D, Entman ML. Fc Receptor Engagement Mediates Differentiation of Cardiac Fibroblast Precursor Cells. Proceedings of the National Academy of Sciences. 2008; 105(29):10179–84. https://doi.org/10.1073/pnas.0804910105 PMID: 18632582

30. Murray LA, Rosada R, Moreira AP, Joshi A, Kramer MS, Hesson DP, et al. Serum Amyloid P Therapeutically Attenuates Murine Bleomycin-Induced Pulmonary Fibrosis via Its Effects on Macrophages. PLOS ONE. 2010; 5(3):e9683. https://doi.org/10.1371/journal.pone.0009683 PMID: 20300636

31. Murray LA, Chen Q, Kramer MS, Hesson DP, Argentieri RL, Peng X, et al. TGF-beta driven lung fibrosis is macrophage dependent and blocked by Serum amyloid P. Int J Biochem Cell Biol. 2011; 43(1):154–62. Epub 2010/11/04. https://doi.org/10.1016/j.biocel.2010.10.013 PMID: 21044893.

32. Castaño AP, Lin S-L, Surowy T, Nowlin BT, Turlapati SA, Patel T, et al. Serum Amyloid P Inhibits Fibrosis Through FcγR-Dependent Monocyte-Macrophage Regulation in Vivo. Science Translational Medicine. 2009; 1(5):5ra13.

33. Pilling D, Fan T, Huang D, Kaul B, Gomer RH. Identification of markers that distinguish monocyte-derived fibrocytes from monocytes, macrophages, and fibroblasts. PLoS One. 2009; 4(10):e7475. Epub 2009/10/17. https://doi.org/10.1371/journal.pone.0007475 PMID: 19834619.

34. Karhadkar TR, Pilling D, Cox N, Gomer RH. Sialidase inhibitors attenuate pulmonary fibrosis in a mouse model. Scientific Reports. 2017; 7(1):15069. https://doi.org/10.1038/s41598-017-15198-8 PMID: 29118338

35. Reyfman PA, Walter JM, Joshi N, Anekalla KR, McQuattie-Pimentel AC, Chiu S, et al. Single-Cell Transcriptomic Analysis of Human Lung Provides Insights into the Pathobiology of Pulmonary Fibrosis. Am J Respir Crit Care Med. 2018. Epub 2018/12/18. https://doi.org/10.1164/rccm.201712-2410OC PMID: 30554520.

36. Nakagawa N, Barron L, Gomez IG, Johnson BG, Roach AM, Kameoka S, et al. Pentraxin-2 suppresses c-Jun/AP-1 signaling to inhibit progressive fibrotic disease. JCI Insight. 2016; 1(20). https://doi.org/10.1172/jci.insight.87446 PMID: 27942582

37. Zhang YM, Fang YD, Wang YC, Wang SL, Lei ZY, Liu XW, et al. Role of serum amyloid P in skin graft survival and wound healing in burned patients receiving skin grafts. Clin Chim Acta. 2011; 412:227–9. Epub 2010/10/12. https://doi.org/10.1016/j.cca.2010.09.036 PMID: 20932823.

38. Galkina EV, Nazarov PG, Polevschikov AV, Berestovaya LK, Galkin VE, Bychkova NV. Interactions of C-Reactive Protein and Serum Amyloid P Component with Interleukin-8 and Their Role in Regulation of Neutrophil Functions. Russ J Immunol. 2000; 5(4):363–74. Epub 2003/04/11. PMID: 12687191.

39. Stibenz D, Grafe M, Debus N, Hasbach M, Bahr I, Graf K, et al. Binding of human serum amyloid P component to L-selectin. Eur J Immunol. 2006; 36(2):446–56. Epub 2006/01/20. https://doi.org/10.1002/eji.200425360 PMID: 16421944.

40. Herlihy SE, Pilling D, Maharjan AS, Gomer RH. Dipeptidyl Peptidase IV Is a Human and Murine Neutrophil Chemorepellent. The Journal of Immunology. 2013; 190(12):6468–77. https://doi.org/10.4049/jimmunol.1202583 PMID: 23677473

41. Cong M, Zhao W, Liu T, Wang P, Fan X, Zhai Q, et al. Protective effect of human serum amyloid P on CCl4-induced acute liver injury in mice. International journal of molecular medicine. 2017; 40(2):454–64. Epub 2017/06/20. https://doi.org/10.3892/ijmm.2017.3028 PMID: 28627620.

42. Verstovsek S, Manshouri T, Pilling D, Bueso-Ramos CE, Newberry KJ, Prijic S, et al. Role of neoplastic monocyte-derived fibrocytes in primary myelofibrosis. J Exp Med. 2016; 213(9):1723–40. Epub 2016/08/03. https://doi.org/10.1084/jem.20160283 PMID: 27481130.

43. Raghu G, Remy-Jardin M, Myers JL, Richeldi L, Ryerson CJ, Lederer DJ, et al. Diagnosis of Idiopathic Pulmonary Fibrosis. An Official ATS/ERS/JRS/ALAT Clinical Practice Guideline. Am J Respir Crit Care Med. 2018; 198(5):e44–e68. Epub 2018/09/01. https://doi.org/10.1164/rccm.201807-1255ST PMID: 30168753.

44. Job ER, Bottazzi B, Gilbertson B, Edenborough KM, Brown LE, Mantovani A, et al. Serum Amyloid P Is a Sialylated Glycoprotein Inhibitor of Influenza A Viruses. PLoS ONE. 2013; 8(3):e59623. https://doi.org/10.1371/journal.pone.0059623 PMID: 23544079

45. Andersen O, Vilsgaard Ravn K, Juul Sorensen I, Jonson G, Holm Nielsen E, Svehag SE. Serum amyloid P component binds to influenza A virus haemagglutinin and inhibits the virus infection in vitro. Scand J Immunol. 1997; 46(4):331–7. Epub 1997/11/14. https://doi.org/10.1046/j.1365-3083.1997.d01-147.x PMID: 9350282.

46. Horvath A, Andersen I, Junker K, Lyck Fogh-Schultz B, Holm Nielsen E, Gizurarson S, et al. Serum amyloid P component inhibits influenza A virus infections: in vitro and in vivo studies. Antiviral Res. 2001; 52(1):43–53. Epub 2001/09/01. https://doi.org/10.1016/s0166-3542(01)00158-9 PMID: 11530187.

47. Li Y, Chen M, Cao H, Zhu Y, Zheng J, Zhou H. Extraordinary GU-rich single-strand RNA identified from SARS coronavirus contributes an excessive innate immune response. Microbes and infection. 2013; 15(2):88–95. Epub 2012/11/06. https://doi.org/10.1016/j.micinf.2012.10.008 PMID: 23123977.

48. Majer O, Liu B, Barton GM. Nucleic acid-sensing TLRs: trafficking and regulation. Current opinion in immunology. 2017; 44:26–33. Epub 2016/11/28. https://doi.org/10.1016/j.coi.2016.10.003 PMID: 27907816.

49. Heil F, Hemmi H, Hochrein H, Ampenberger F, Kirschning C, Akira S, et al. Species-specific recognition of single-stranded RNA via toll-like receptor 7 and 8. Science. 2004; 303(5663):1526–9. Epub 2004/02/21. https://doi.org/10.1126/science.1093620 PMID: 14976262.

50. Shao DD, Suresh R, Vakil V, Gomer RH, Pilling D. Pivotal Advance: Th-1 cytokines inhibit, and Th-2 cytokines promote fibrocyte differentiation. J Leukoc Biol. 2008; 83(6):1323–33. Epub 2008/03/12. https://doi.org/10.1189/jlb.1107782 PMID: 18332234.

51. Daubeuf F, Frossard N. Performing Bronchoalveolar Lavage in the Mouse. Current protocols in mouse biology. 2012; 2(2):167–75. Epub 2012/01/01. https://doi.org/10.1002/9780470942390.mo110201 PMID: 26069010.

52. Walters DM, Kleeberger SR. Mouse models of bleomycin-induced pulmonary fibrosis. Current protocols in pharmacology. 2008;Chapter 5:Unit 5.46. Epub 2008/03/01. https://doi.org/10.1002/0471141755.ph0546s40 PMID: 22294226.

53. Pilling D, Kitas GD, Salmon M, Bacon PA. The kinetics of interaction between lymphocytes and magnetic polymer particles. Journal Of Immunological Methods. 1989; 122:235–41. 43. https://doi.org/10.1016/0022-1759(89)90269-x PMID: 2794518

54. Pilling D, Zheng Z, Vakil V, Gomer RH. Fibroblasts secrete Slit2 to inhibit fibrocyte differentiation and fibrosis. Proceedings of the National Academy of Sciences of the United States of America. 2014; 111(51):18291–6. Epub 2014/12/10. https://doi.org/10.1073/pnas.1417426112 PMID: 25489114.

55. Karhadkar TR, Chen W, Gomer RH. Attenuated pulmonary fibrosis in sialidase-3 knockout (Neu3-/-) mice. American Journal of Physiology-Lung Cellular and Molecular Physiology. 2020: 318(1): p. L165–L79. https://doi.org/10.1152/ajplung.00275.2019 PMID: 31617733

56. Donovan J, Brown P. Blood Collection. Current Protocols in Neuroscience. 2005; 33(1):A.4G.1–A.4G.9. https://doi.org/10.1002/0471142301.nsa04gs33 PMID: 18428617

57. Parasuraman S, Raveendran R, Kesavan R. Blood sample collection in small laboratory animals. J Pharmacol Pharmacother. 2010; 1(2):87–93. https://doi.org/10.4103/0976-500X.72350 PMID: 21350616.

58. Pilling D, Gomer RH. Persistent Lung Inflammation and Fibrosis in Serum Amyloid P Component (Apcs-/-) Knockout Mice. PLOS ONE. 2014; 9(4):e93730. https://doi.org/10.1371/journal.pone.0093730 PMID: 24695531

59. Faul F, Erdfelder E, Buchner A, Lang A-G. Statistical power analyses using G*Power 3.1: Tests for correlation and regression analyses. Behavior Research Methods. 2009; 41(4):1149–60. https://doi.org/10.3758/BRM.41.4.1149 PMID: 19897823

60. Faul F, Erdfelder E, Lang A-G, Buchner A. G*Power 3: A flexible statistical power analysis program for the social, behavioral, and biomedical sciences. Behavior Research Methods. 2007; 39(2):175–91. https://doi.org/10.3758/bf03193146 PMID: 17695343

61. Bhide GP, Colley KJ. Sialylation of N-glycans: mechanism, cellular compartmentalization and function. Histochemistry and cell biology. 2017; 147(2):149–74. Epub 2016/12/16. https://doi.org/10.1007/s00418-016-1520-x PMID: 27975143.

62. Linkins L-A, Takach Lapner S. Review of D-dimer testing: Good, Bad, and Ugly. International Journal of Laboratory Hematology. 2017; 39(S1):98–103. https://doi.org/10.1111/ijlh.12665.

63. Schutgens RE. D-dimer in COVID-19: A Guide With Pitfalls. Hemasphere. 2020; 4(4):e422–e. https://doi.org/10.1097/HS9.0000000000000422 PMID: 32904041.

64. Yao Y, Cao J, Wang Q, Shi Q, Liu K, Luo Z, et al. D-dimer as a biomarker for disease severity and mortality in COVID-19 patients: a case control study. Journal of Intensive Care. 2020; 8(1):49. https://doi.org/10.1186/s40560-020-00466-z PMID: 32665858

65. Kuri-Cervantes L, Pampena MB, Meng W, Rosenfeld AM, Ittner CAG, Weisman AR, et al. Comprehensive mapping of immune perturbations associated with severe COVID-19. Sci Immunol. 2020; 5(49). Epub 2020/07/17. https://doi.org/10.1126/sciimmunol.abd7114 PMID: 32669287.

66. Schulte-Schrepping J, Reusch N, Paclik D, Baßler K, Schlickeiser S, Zhang B, et al. Severe COVID-19 is marked by a dysregulated myeloid cell compartment. Cell. 2020. https://doi.org/10.1016/j.cell.2020.08.001 PMID: 32810438

67. Wilk AJ, Rustagi A, Zhao NQ, Roque J, Martínez-Colón GJ, McKechnie JL, et al. A single-cell atlas of the peripheral immune response in patients with severe COVID-19. Nature Medicine. 2020; 26(7):1070–6. https://doi.org/10.1038/s41591-020-0944-y PMID: 32514174

68. Giamarellos-Bourboulis EJ, Netea MG, Rovina N, Akinosoglou K, Antoniadou A, Antonakos N, et al. Complex Immune Dysregulation in COVID-19 Patients with Severe Respiratory Failure. Cell Host Microbe. 2020; 27(6):992–1000.e3. Epub 2020/04/23. https://doi.org/10.1016/j.chom.2020.04.009 PMID: 32320677.

69. Sánchez-Cerrillo I, Landete P, Aldave B, Sánchez-Alonso S, Sánchez-Azofra A, Marcos-Jiménez A, et al. COVID-19 severity associates with pulmonary redistribution of CD1c+ DC and inflammatory transitional and nonclassical monocytes. The Journal of Clinical Investigation. 2020. https://doi.org/10.1172/JCI140335 PMID: 32784290

70. Vannella KM, Wynn TA. Mechanisms of Organ Injury and Repair by Macrophages. Annu Rev Physiol. 2017; 79:593–617. Epub 2016/12/14. https://doi.org/10.1146/annurev-physiol-022516-034356 PMID: 27959618.

71. Mould KJ, Barthel L, Mohning MP, Thomas SM, McCubbrey AL, Danhorn T, et al. Cell Origin Dictates Programming of Resident versus Recruited Macrophages during Acute Lung Injury. American journal of respiratory cell and molecular biology. 2017; 57(3):294–306. https://doi.org/10.1165/rcmb.2017-0061OC PMID: 28421818.

72. UniProt Consortium T. UniProt: the universal protein knowledgebase. Nucleic Acids Res. 2018; 46(5):2699. Epub 2018/02/10. https://doi.org/10.1093/nar/gky092 PMID: 29425356.

73. Crawford JR, Pilling D, Gomer RH. Improved serum-free culture conditions for spleen-derived murine fibrocytes. Journal of immunological methods. 2010; 363(1):9–20. Epub 2010/10/05. https://doi.org/10.1016/j.jim.2010.09.025 PMID: 20888336.

74. Naik-Mathuria B, Pilling D, Crawford JR, Gay AN, Smith CW, Gomer RH, et al. Serum amyloid P inhibits dermal wound healing. Wound Repair and Regeneration. 2008; 16(2):266–73. https://doi.org/10.1111/j.1524-475X.2008.00366.x PMID: 18318811

75. Murray L, Kramer M, Hesson D, Watkins B, Fey E, Argentieri R, et al. Serum amyloid P ameliorates radiation-induced oral mucositis and fibrosis. Fibrogenesis & Tissue Repair. 2010; 3(1):11. https://doi.org/10.1186/1755-1536-3-11 PMID: 20602770

76. Vivier E, Artis D, Colonna M, Diefenbach A, Di Santo JP, Eberl G, et al. Innate Lymphoid Cells: 10 Years On. Cell. 2018; 174(5):1054–66. Epub 2018/08/25. https://doi.org/10.1016/j.cell.2018.07.017 PMID: 30142344.

77. Barlow JL, McKenzie ANJ. Innate Lymphoid Cells of the Lung. Annual Review of Physiology. 2019; 81(1):429–52. https://doi.org/10.1146/annurev-physiol-020518-114630 PMID: 30742786

78. Willinger T. Metabolic Control of Innate Lymphoid Cell Migration. Frontiers in immunology. 2019; 10:2010-. https://doi.org/10.3389/fimmu.2019.02010 PMID: 31507605.

79. McElvaney OJ, McEvoy N, McElvaney OF, Carroll TP, Murphy MP, Dunlea DM, et al. Characterization of the Inflammatory Response to Severe COVID-19 Illness. American Journal of Respiratory and Critical Care Medicine. 2020. https://doi.org/10.1164/rccm.202005-1583OC PMID: 32584597

80. Chen W, Lamb TM, Gomer RH. TGF-β1 increases sialidase 3 expression in human lung epithelial cells by decreasing its degradation and upregulating its translation. Experimental Lung Research. 2020; 46 (3–4):75–80. https://doi.org/10.1080/01902148.2020.1733135 PMID: 32102576

81. Bagri P, Anipindi VC, Nguyen PV, Vitali D, Stämpfli MR, Kaushic C. Novel Role for Interleukin-17 in Enhancing Type 1 Helper T Cell Immunity in the Female Genital Tract following Mucosal Herpes Simplex Virus 2 Vaccination. Journal of Virology. 2017; 91(23):e01234–17. https://doi.org/10.1128/JVI.01234-17 PMID: 28956763

82. Scharff AZ, Rousseau M, Lacerda Mariano L, Canton T, Consiglio CR, Albert ML, et al. Sex differences in IL-17 contribute to chronicity in male versus female urinary tract infection. JCI Insight. 2019; 4(13). https://doi.org/10.1172/jci.insight.122998 PMID: 31145099

83. Khalil N, O'Connor R. The Role of TGF-β in Bleomycin Induced Pulmonary Fibrosis. In: Jakowlew SB, editor. Transforming Growth Factor-β in Cancer Therapy, Volume I: Basic and Clinical Biology. Totowa, NJ: Humana Press; 2008. p. 581–94.

84. Luzina IG, Lockatell V, Hyun SW, Kopach P, Kang PH, Noor Z, et al. Elevated expression of NEU1 sialidase in idiopathic pulmonary fibrosis provokes pulmonary collagen deposition, lymphocytosis, and fibrosis. American journal of physiology Lung cellular and molecular physiology. 2016; 310(10):L940–54. Epub 2016/03/20. https://doi.org/10.1152/ajplung.00346.2015 PMID: 26993524.

85. Barnes PJ. Sex Differences in Chronic Obstructive Pulmonary Disease Mechanisms. American Journal of Respiratory and Critical Care Medicine. 2016; 193(8):813–4. https://doi.org/10.1164/rccm.201512-2379ED PMID: 27082528.